Journal of Agrometeorology 3(1&2) : 237-260 (June-December 2001)

Planetary boundary layer structure during February and May, over a semi-arid station - A numerical simulation

A. K. DAS, U. C. MOHANTY*, A. N. V. SATYANARAYANA AND A. SARKAR[1]

Centre for Atmospheric Sciences, IIT, Hauz Khas, New Delhi - 110 016.

[1] Modi College of Engineering and Technology, Lakshamangarh, Sikar, Rajasthan

ABSTRACT

Two-dimensional version of a high-resolution non-hydrostatic mesoscale model namely ARPS (Advanced Regional Prediction System) was used to simulate the Planetary Boundary Layer (PBL) processes over a semi-arid region of western India. Intensive observational data during two different seasons viz. winter and summer (February and May) were collected from the Land Surface Processes Experiment (LASPEX-97), conducted at Anand (22°35'N, 72°55'E) during 1997 over Sabarmati Basin Gujarat. A comparative study of three subgrid-scale turbulence parameterization schemes was conducted to find out the most suitable scheme. The model generated vertical profiles (zonal and meridional wind components, potential temperature and specific humidity) were validated against available observations bringing out the significant characteristics of thermal structure and circulation pattern in the PBL. Diurnal variation of surface and soil temperature, net radiation, sensible, latent and soil heat flux distinguish the surface response during two different seasons. Besides, the study of temporal variation of turbulent kinetic energy (TKE) from model simulation facilitates the understanding of the characteristics of the PBL structure.

Key words : PBL, TKE, ARPS, Numerical Simulation

The success of Planetary Boundary Layer (PBL) research depends on the computational power and sufficient observational experiments to support. The understanding of the structure of the PBL has made significant advances in recent years with the exponential increase of computing power. On the experimental front also the progress is convincing all over the globe. Several investigators studied PBL characteristics utilising different models through observational experiments (e.g. Yamada, 1976, Caughey *et al.* 1979, Noilhan *et al.*, 1991, Potty, *et al.*, 1995). Comparison and validation of turbulence closure schemes regarding atmospheric phenomena are also done by several researchers (e.g. Holt *et al.*, 1988, Chorbok *et al.*, 1992, Musson-Genon, 1995). Very few studies were conducted to study the land surface processes (LSP) and its impact on PBL structure over a semi-arid tropical region in India. Satyanarayana *et al.* (2000) studied the atmospheric boundary layer over Anand during winter by employing a multi-level PBL model with soil heat and moisture transport scheme. Further, mesoscale model results and different PBL schemes also have not been validated against observations over this region. In this paper, seasonal variation in PBL characteristics are studied

* **Corresponding Author:** e-mail- mohanty@cas.iitd.ernet.in

utilising observational data of Land Surface Processes Experiment (LASPEX-97) conducted by Indian Institute of Tropical Meteorology (IITM), Pune and Gujarat Agriculture University, Anand, in the semi-arid sub-tropical region of Gujarat in India.

MATERIALS AND METHODS

The Advanced Regional Prediction System (ARPS) has been developed at the Centre for Analysis and Prediction of Storms (CAPS) at the University of Oklahoma, USA is a 3-dimensional, non-hydrostatic, compressible model formulated in generalised terrain-following co-ordinate system. This can be run as a 1-2 dimensional model with governing equations involving minimum approximations. The model employs different physical parameterisation schemes that are important for explicit prediction of small-scale systems as well as the flows on larger scales through a feedback mechanism provided in the model.

The governing equations of ARPS

The governing equations of the ARPS include those of conservation of momentum, heat, water substance, subgrid scale (SGS) Turbulence Kinetic Energy (TKE) along with the equation of state for moist air (Ming *et al.*, 1995). Among the three state variable (temperature, pressure and density) prognostic equations for two of them are established for prediction and the 3rd variable is diagnosed. Potential temperature and pressure are chosen for prediction and then density is diagnosed. In the closed system the surface pressure is first predicted to express the pressure gradient force (PGF) directly in the form as it is in the Navier-Stokes equations.

In ARPS, governing equations are first expressed in the Cartesian co-ordinate system (Haltiner *et al.*, 1980). In the closed system the governing equations are formulated in a curvilinear co-ordinate system (ξ,η,ζ) defined by

$\xi = \xi(x)$,

$\eta = \eta(y)$ and

$\zeta = \zeta(x,y,z)$

The constant surfaces of x and h remain parallel to constant x and y, while the vertical transformation allows grid-stretching and ensures that the lower boundary conforms to the terrain. In the computational domain the transformation thus maps a domain with stretched vertical grid and an irregular lower boundary, to a regular rectangular domain with equal grid spacing in each direction. Cartesian velocity components u,v and w are expressed as functions of the contravariant velocity components U^c, V^c and W^c (Sharman *et al.*, 1988). The transformation relations for spatial derivatives from (x,y,z) to (ξ,η,ζ) are expressed in terms of Jacobians (Ming *et al.*, 1995) and calculated numerically in the model. The final model equations are obtained through perturbation techniques as in the non-hydrostatic models. The atmospheric state variables are divided into a basic state independent of x and y and a perturbation varying in all directions. An overview of the ARPS model and its domain are given in Table 1 and 2 within Appendix.

The numerical solution

(a) Basic dicretization :

The continuous model equations are solved using finite differences on an Arakawa C-grid (Arakawa *et al.*, 1977). All prognostic variables are defined at the centre of the grid

Table 1 : Overview of the ARPS Model (version 4.4.0)

Model	Advanced Regional Prediction System (ARPS)
Dynamics	• Non-hydrostatic
Prognostic variables	u,v,w,θ', p' and q (q_v, q_c, q_r) Basic State : Hydrostatic
Domain	• User specified
Number of horizontal grid points	
Horizontal resolution	
Number of vertical levels	
Horizontal grid system	• Arakawa C-grid (Arakawa *et al.*, 1977)
Vertical coordinate	• Terrain following Z coordinate
Time scheme	• Large time step: Leap frog scheme with mode splitting technique (Klemp *et al.*, 1978) • Small time step: Crank-Nicolson Scheme
Spatial Differencing	• Finite difference (2nd and 4th order)
Lateral boundary condition	• Rigid wall • Periodic • Zero gradient • Open radiative on all four sides of the domain (Durran *et al.*, 1983) • External forced lateral boundary • Nested grid lateral boundary
Top boundary condition	• Rigid wall • Periodic • Zero gradient • Linear hydrostatic radiative (Chen, 1991) (in this study)
Bottom Boundary	• Rigid wall
Sub-grid scale turbulent mixing - options :	• Constant mixing co-efficient • Smagorinsky mixing co-efficient (Smagornisky, 1963) • Smagorinsky mixing co-efficient plus a constant co-efficient • 1.5 TKE closure mixing (Moeng *et al.*, 1984) • 1.5 TKE closure mixing (Deardroff, 1980) • 1.5 TKE closure mixing (Sun *et al.*, 1986)
Land surface processes	• Soil-vegetation scheme (Noilhan *et al.*, 1989, Pleim *et al.*, 1995)
Radiation - options :	• Simplified surface radiation : Short wave (Chau, 1992), Long wave (Chau *et al.*, 1994) • Atmospheric radiation transfer
Surface layer parameterisation	• Surface fluxes are calculated from constant surface drag coefficients • Surface fluxes are calculated from the stability-dependent surface drag coefficients • Surface fluxes are calculated from the stability-dependent surface drag coefficients, and predicted surface temperature and surface volumetric water content instead of user specified values.
Cumulus Parameterisation	• Kuo (1965) • Kuo-Kessler (Kuo, 1974) • Kain-Fritsch (Kain *et al.*, 1990)
Micro physics	• Kessler warm rain microphysics (Kessler, 1969) • Ice microphysics (Lin *et al.*, 1983) • NEM ice microphysics (Schultz, 1995)

Table 2 : Model domain description

Experiment No	Model Domain	No of grid points in x direction	No of grid points in z direction	The grid distance in x direction(km)	The grid spacing in z direction(m)
1	x-z plane	151	63	2.5	50
2	x-z plane	151	70	2.5	50

box while the normal velocity components are defined on their respective box faces. Standard spatial averaging and central space differencing is used for all dependent variables

(b) Time integration:

A mode-splitting time integration scheme (Klemp *et al.*, 1978) is employed to integrate the dynamic equations. This technique divides a large time step of integration into a number of small time steps and updates the acoustically active terms at every small time step while computing all other terms only once with a large time step. The large time-step integration uses three-level leapfrog time differencing scheme. The small time-step integration is used with a fully explicit forward-backward scheme or with the vertically implicit Crank-Nicolson scheme. The equations for water substances and TKE are solved entirely on large time step.

Subgrid-scale turbulence

Turbulence parameterisation has the closure link between the resolved scales and unresolved subgrid-scale. In ARPS, several subgrid-scale closure options for turbulent mixing are available. In the context of this paper the following four options are utilised.

(i) the first order closure of Smagorinsky/ Lilly scheme (Smagorinsky, 1963; Lilly, 1962)

(ii) the 1.5 order TKE-based scheme developed by Deardroff (1980)

(iii) the 1.5 order TKE-based scheme of Moeng and Wyngaard (Moeng *et al.*, 1984)

(iv) an ensemble turbulence closure scheme of Sun and Chang (Sun *et al.*, 1986)

Physical processes

A soil-vegetation model (Noilhan *et al.*, 1989; Pleim *et al.*, 1995) is used to predict the time-dependent state of the land surface. In ARPS, the Kessler warm-rain scheme (Kessler, 1969), ice microphysics (Lin *et al.*, 1983) and Schultz NEM scheme (Schultz, 1995) are available for the precipitation processes. Options for convective cumulus parameterisation are modified Kuo scheme (Kuo, 1974) and Kain and Fritsch cumulus parameterisation (Kain *et al.*, 1990). Radiation parameterisation schemes in the ARPS are based on the models of Chau(1992) for short wave and Chau and Suarez (Chau *et al.*, 1994) for long-wave.

Boundary conditions

In ARPS, different types of boundary conditions are available for the lateral, top and bottom boundaries. The following boundary condition options are used in the present study.

(a) *Lateral Boundary :* Open radiative boundary condition is used for all 4-sides of the model domain. This is based on the scheme suggested by Durran and Klemp (Durran *et al.*, 1983).

(b) *Top Boundary :* Linear hydrostatic radiation boundary is considered following Chen (Chen, 1991).

(c) *Bottom Boundary :* The bottom of the model domain is considered as a rigid wall.

Data

A multi-stational land surface processes experiment (LASPEX-97) during 1997 was conducted at five locations (Anand, Khandha, Arnej, Derol and Sanand) in the Sabarmati Basin of Gujarat in India. For the present study, micro-meteorological tower data consisting of wind speed, wind direction and temperature at 4 different heights (1, 2, 4 and 8 m) collected at Anand (22.4°N, 72.6°E) are used. Sonic anemometer measurements gave continuous data for wind speed and wind direction, temperature and relative humidity. Sensible heat flux was directly measured by Metek anemometer. Various soil parameters (e.g. texture, soil type, soil temperature and moisture) and vegetation parameters (e.g. vegetation cover, leaf area index) are used in the model. RS/RW data provided vertical profiles of wind speed and direction, temperature and relative humidity at different pressure levels, which facilitated the study of turbulent characteristics of PBL.

Numerical experiments

Round the clock data of one winter day (0300 UTC of 14th - 0300 UTC of 15th February) and a summer day (0300 UTC of 13th - 0300 UTC of 14th May) at Anand are considered for simulation. In two numerical experiments, model integration was carried out synthesizing hourly surface data with 6 hourly rawinsonde data at Anand. Simulations are carried out with all the four different closure options mentioned earlier keeping other physical conditions in the model unaltered.

Initial conditions

Observed vertical profiles of potential temperature, wind and specific humidity are taken for model initialisation. Surface pressure, surface temperature, deep soil temperature, surface soil moisture and deep soil moisture are specified from the observed data. Initial time for the simulations is specified according to the time of RS/RW ascent viz. experiment 1 - 0300 UTC 14 February, 1997 and experiment 2- 0300 UTC 13 May, 1997.

RESULTS AND DISCUSSION

Analysis was done on two different aspects. (i) to see the model response in describing the general PBL characteristics in two contrasting seasons, winter and summer and (ii) to study model performance with different subgrid-scale turbulence parameterisation schemes.

The simulated and the corresponding observed vertical profiles of potential temperature at 06 and 09 UTC of 14 February and 00 and 03 UTC of 15 February (winter), 1997 are shown in Fig. 1(a-d). Fig.1(a) shows the development of an inversion layer near

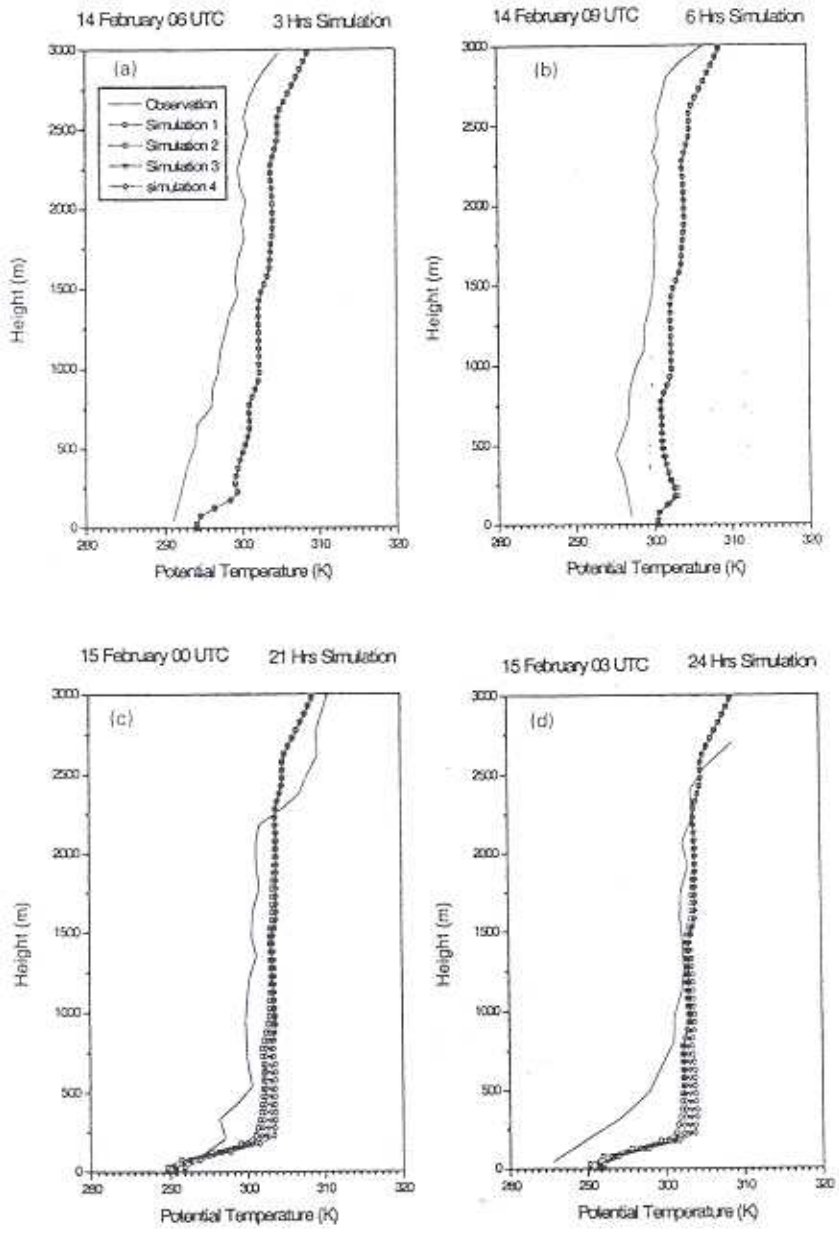

Fig. 1 : Potential temperature profiles - observed and simulated on 14 and 15 February, 1997 at a) 3 hrs, b) 6 hrs, c) 21 hrs and d) 24 hrs of simulation.

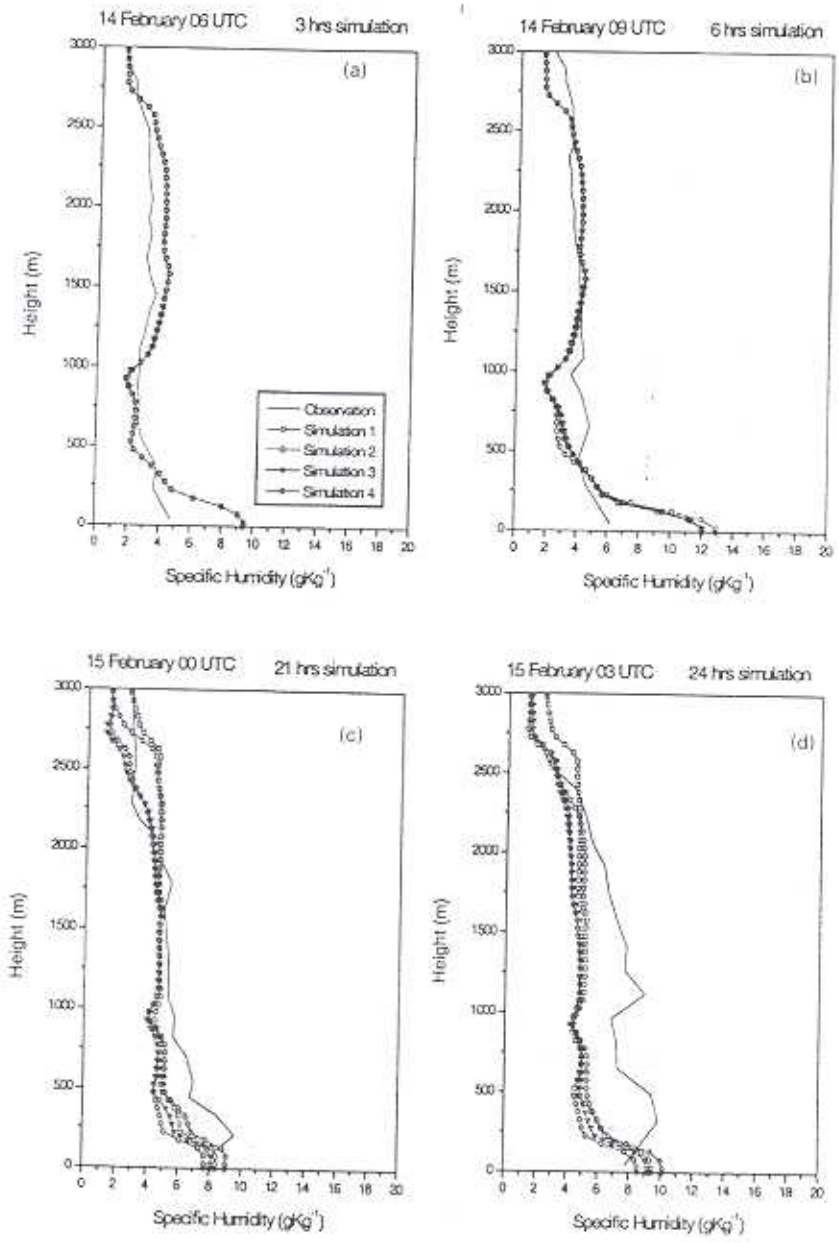

Fig. 2 : Specific humidity profiles - observed and simulated on 14 and 15 February, 1997 at a) 3 hrs, b) 6 hrs, c) 21 hrs and d) 24 hrs of simulation.

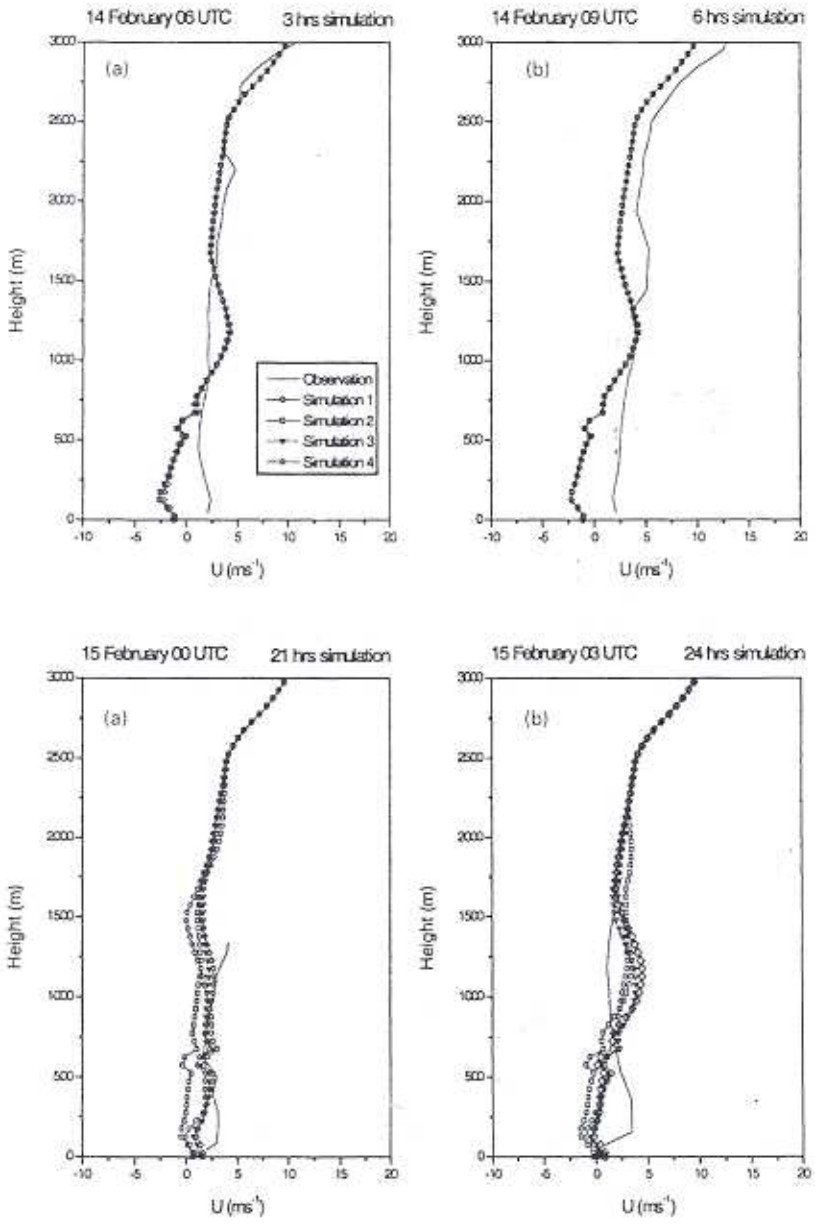

Fig. 3 : Profiles of zonal-wind component - observed and simulated on 14 and 15 February, 1997 at a) 3 hrs, b) 6 hrs, c) 21 hrs and d) 24 hrs of simulation.

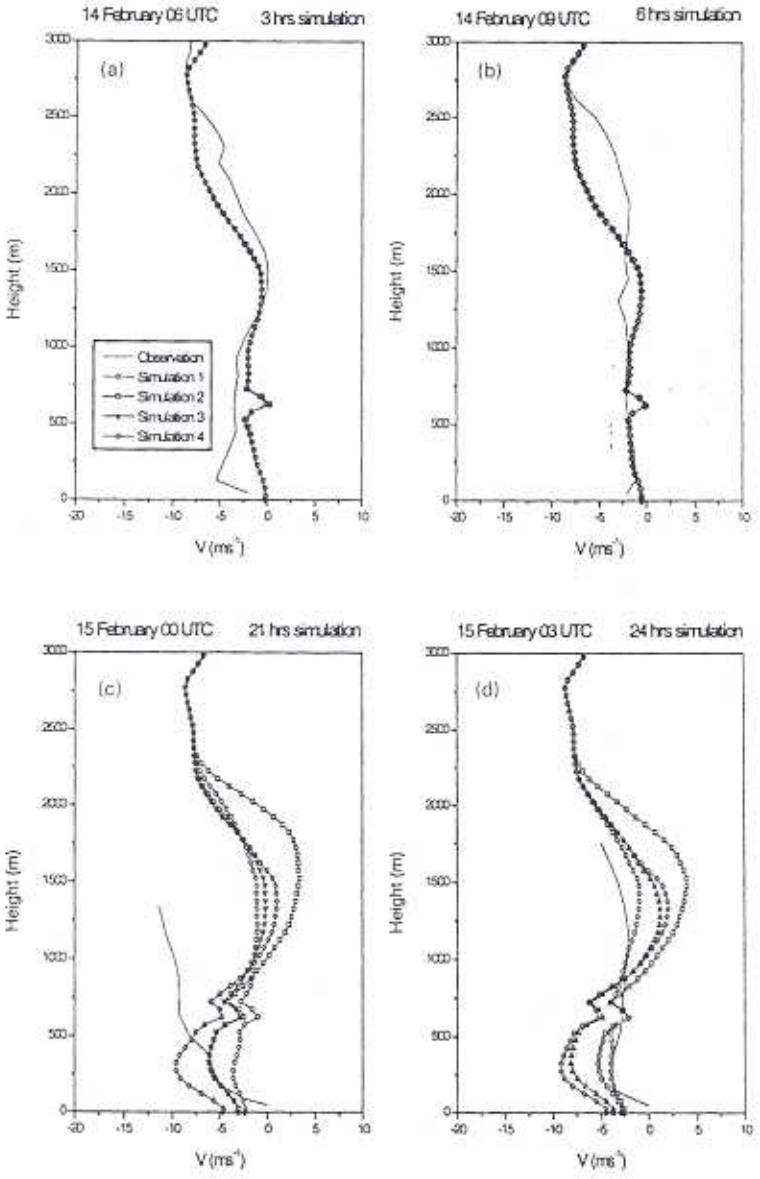

Fig. 4 : Profiles of meridional wind component - observed and simulated on 14 and 15 February, 1997 at a) 3 hrs, b) 6 hrs, c) 21 hrs and d) 24 hrs of simulation.

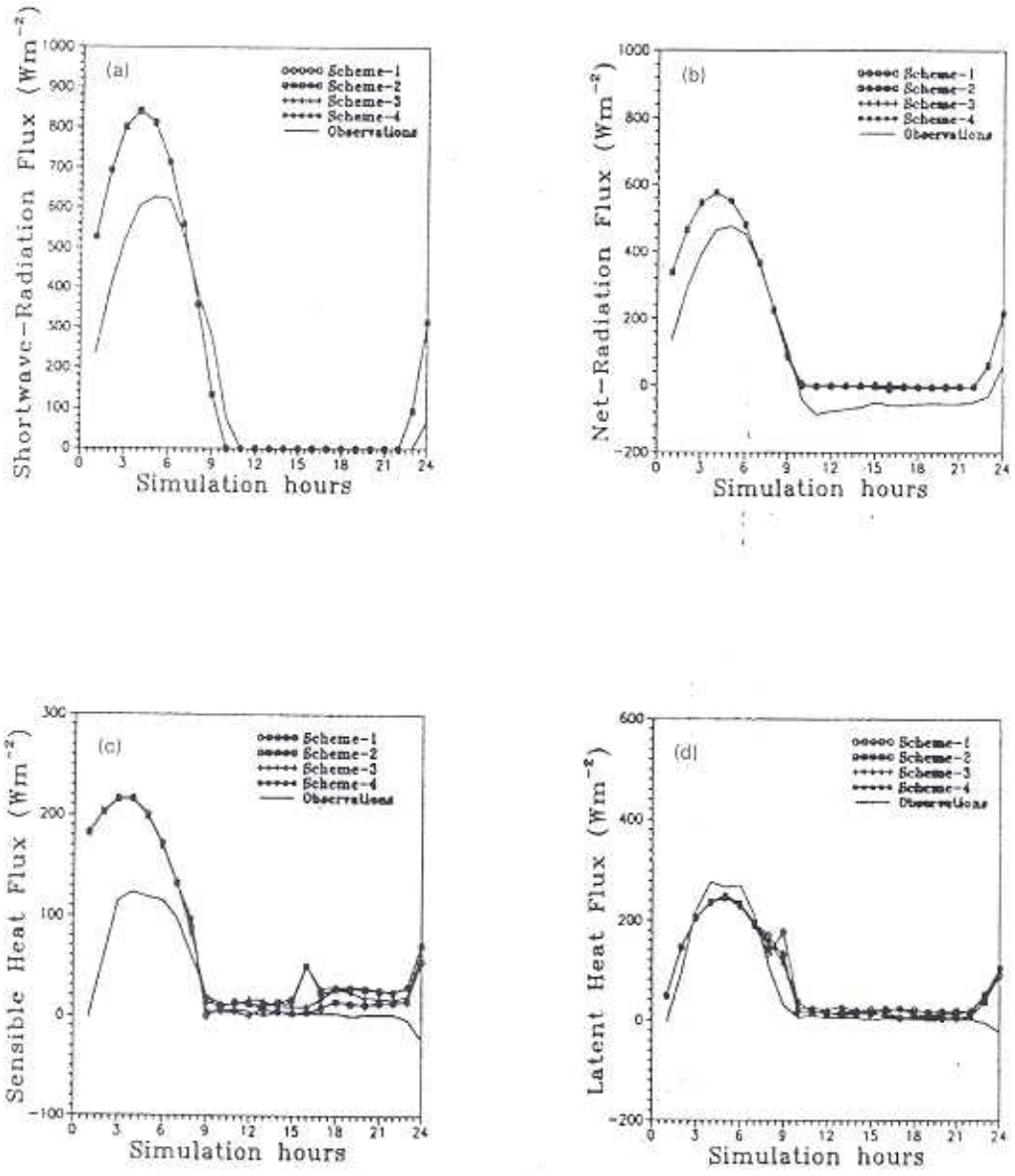

Fig 5 : Diurnal variation of energy fluxes at surface (a) short wave radiation, (b) net radiation (c) sensible heat and (d) letent heat starting from 03 UTC 14 February to 03 UTC 15 February, 1997.

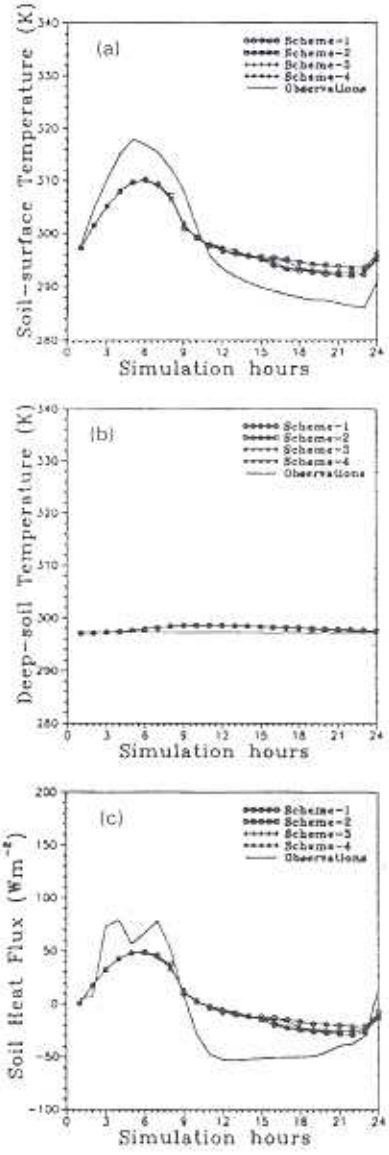

Fig. 6 : Diurnal variation of (a) soil surface temperature, (b) deep-soil temperature and (c) soil heat flux starting from 03 UTC 14 February to 03 UTC 15 February, 1997.

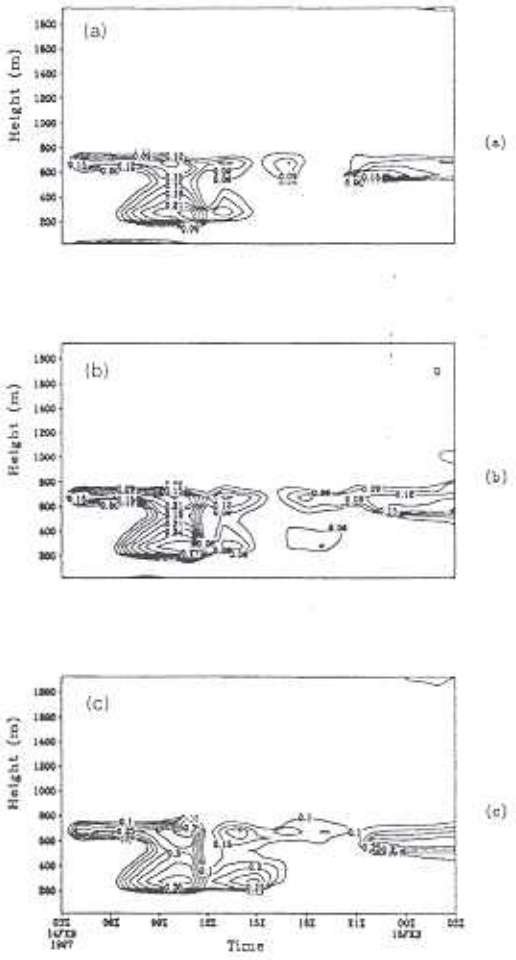

Fig. 7 : The time versus height contour plots of TKE (m^2s^{-1}) with three different subgrid-scale turbulence parameterisation options on 14 and 15 February, 1997. (a) 1.5 order TKE closure scheme of Moeng and Wyngaard, (b) 1.5 order TKE closure scheme of Deardroff and (c) 1.5 order ensemble closure scheme of Sun and Chang.

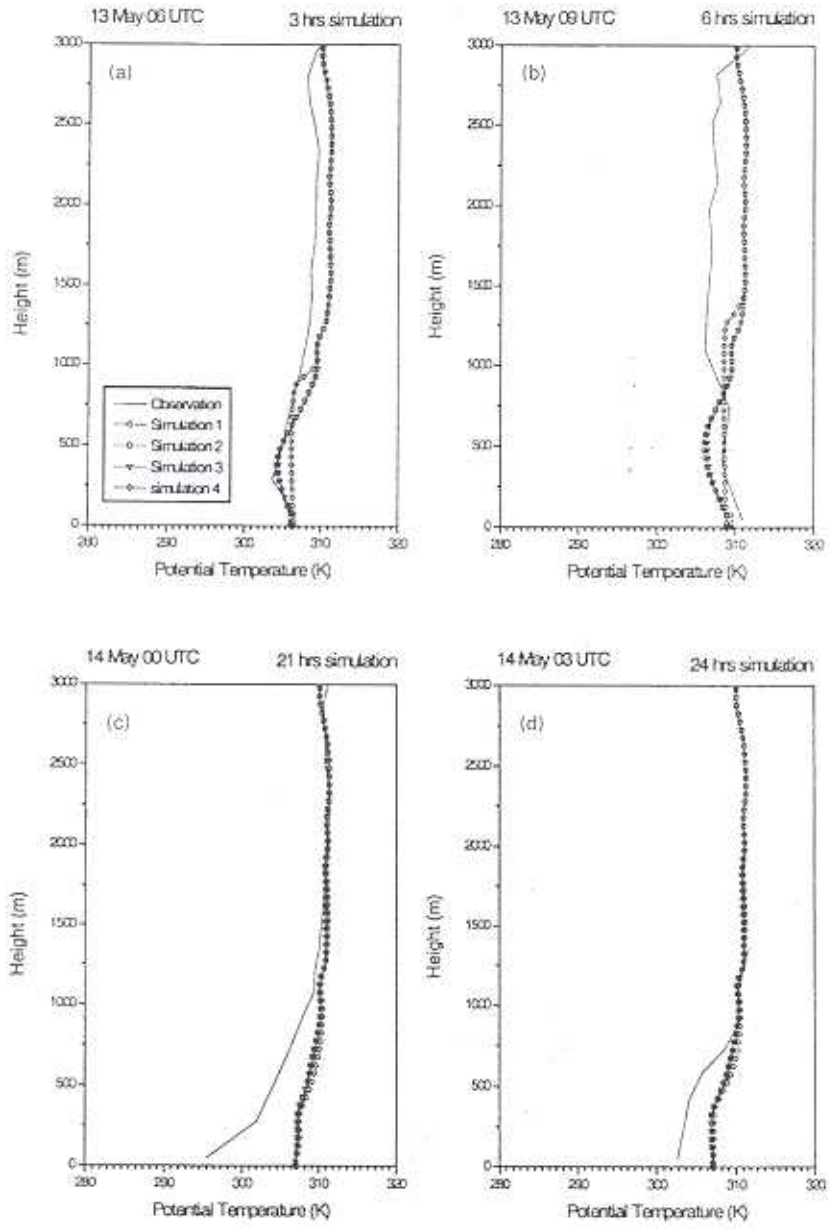

Fig. 8 : Potential temperature profiles - observed and simulated on 13 and 14 May, 1997 at a) 3 hrs, b) 6 hrs, c) 9hrs, d) 21 hrs and e) 24 hrs of simulation.

the surface (up to 300 m Height) after 3 hrs of simulation although it is not present in the observation. Fig.1(b) shows the continuation of this inversion layer even after 6 hrs of simulation. Observations show the development of an unstable layer in the lower levels. Fig.1(c-d) however show the dominance of purely stable layer close to the surface in the early hours of the next day. In general, stably stratified structure of the PBL in the dry period over the dry region is well simulated except during the first few hours of simulation.

The specific humidity profiles at 06 and 09 UTC, 14 February and 00 and 03 UTC 15 February, 1997 are plotted in Fig.2(a-d). In Fig.2(a-b), the amount of moisture decreases very rapidly with height near surface in accordance with potential temperature profiles simulated above. Above 1 km from the surface the model simulated profiles are in good agreement with observations. There is an underestimation of moisture simulated by the model in the early morning (00 UTC and 03 UTC) as shown in Fig.2(c) and 2 (d) as also in the case of potential temperature above.

Fig. 8(a-d) show the potential temperature profiles at 06 and 09 UTC of 13 May and 00 and 03 UTC of 14 May (summer), 1997 respectively. The model simulations for the first 6 hours are showing an unstable layer near the surface and fully stable layer above 1 km in accordance with observations. Model simulations in Fig. 8(c-d) show a stable layer formation above 250 m in the early morning (00 UTC and 03 UTC) as indicated in the observations. Simulations at these hours are however showing near neutral situation near surface, which is a significant departure from the observations. It seems that the cooling process near the soil surface is slowly undergoing in the model. Well above the land surface (above 1 - 1.5 km from the surface) the boundary layer is well mixed for the whole day (13 - 14 May). In general, thermal structure showing the same features as discussed in other study by Nagar *et al.* (2000). Figs. 1 and 8 illustrate that in winter PBL is stable where as in summer it is unstable near surface. The PBL over dry region is distinctly well mixed in both the seasons.

The specific humidity profiles at 06 and 09 UTC of 13 May and 00 and 03 UTC of 14 May, 1997 are shown in Fig. 9(a)-(d). The amount of moisture is high near surface and decreases with height in the model simulation as in the observations except that the model simulations are overestimating near surface as shown in Figs. 9(c) and 9(d). Above 1 km from the surface again the model simulations are overestimating specific humidity (Figs. 9(a-d)). In general, a comparison of Fig. 2 with Fig. 9 indicates that the moisture pattern in PBL changes with season even over a dry region.

The profiles of zonal wind component are shown in Figs. 3 and 10 for the months of February (06, 09 UTC, 14 February and 00, 03 UTC 15 February) and May (06, 09 UTC, 13 May and 00, 03 UTC, 14 May) respectively. Fig.3 shows that in February the magnitude of the zonal wind component is very low (below ± 5 ms^{-1}) up to a height of 2.5 km. The model simulations agree well with observations but are unable to capture the weak westerly zonal wind near the surface. Fig. 10(a-b) show that in May the zonal wind is very weak (below ± 5 ms^{-1}) in magnitude along the whole depth of the PBL except in the early morning within a layer of 500 m above 300 m from the surface (strong westerly exceeding 5 ms^{-1}), that is well presented by model simulations as shown in Fig. 10(c-d).

In Figs. 4 and 11, the profiles of meridional wind component are drawn for the month of February (06, 09 UTC, 14 February and 00, 03 UTC 15 February) and May (06, 09 UTC, 13 May and 00, 03 UTC, 14 May) respectively. Fig.4 (a-b) show that (in February) during the daytime model simulates weak meridional wind up to a height of 1.5 km and fairly strong southerly wind at the top (above 2.5 km) of the PBL but with an exception in the early morning. Fig. 11(a-d) illustrate that in the early morning hours (00UTC and 03 UTC, 14 May) the model simulates well a layer (at 800 m) of high southerly wind whereas a layer (at 750 m) of large meridional wind (southerly) simulated in the day time (03 UTC and 06 UTC, 13 May is absent in observations.

Diurnal variations of short-wave radiation, sensible heat flux, latent heat flux and net radiation for the months of February and May are plotted in Figs. 5 and 12 respectively. In February the model overestimates the maximum of short-wave radiation (Fig. 5). It also shows that the model overestimates the maxima of sensible heat flux and net radiation whereas the minima of net radiation and latent heat flux are very closely underestimated. Fig. 12 shows that in summer month the models predict the short-wave radiation flux well. The maxima and of sensible and latent heat fluxes are underestimated. The model shows higher values for the maxima and the minima of net radiation and latent heat flux compared to observations. Fig. 6 and 13 show that the maxima of soil heat flux are underestimated whereas the minima are overestimated in both the seasons.

Figs.7 and 14 both show the diurnal variation of TKE pattern simulated by the model for the months of February and May respectively. Fig.7 shows that the values of the TKE are very small and the generation of TKE extends up to a height of 800 m. In February, with maximum values (~ 0.3 m^2s^{-1} 200 m and 700 m height. The stratification of the PBL is also prominent in the TKE pattern this. Fig.14 shows the TKE is stronger in the summer month with maximum values (~ 2 m^2s^{-1}) at a height of (100 - 250 m) and TKE generation takes place beyond 1 km from the surface. The model-simulated results of TKE are in qualitative agreement with previous investigators' results (Mellor, *et al.*, 1995).

Thermodynamic structures of the PBL in the model simulations are nearly similar for different SGS parameterisations that are clear in Fig.1 and Fig.8. Only exception is with the scheme of Sun and Chang in the summer month near surface during daytime (Fig.8). The model-simulated results for potential temperature profiles with each closure scheme show a deviation of 2-3 °K from observations near the surface. This is due to the fact that the rate of increase or decrease of surface temperature in the model simulation is rather slow as compared to the real atmosphere, which is shown in Figs.6 and 13. Also the model always underestimates the maximum and underestimates the minimum of the surface temperature. The under prediction of the peak of surface temperature throughout the middle of the day may be raised from too large surface heat capacity in the model. The large amount of moisture in the soil may increase the heat capacity. The under prediction of surface temperature is consistent with the under prediction of soil heat flux, however it is not consistent with the overestimation of sensible heat flux. Comparison of potential

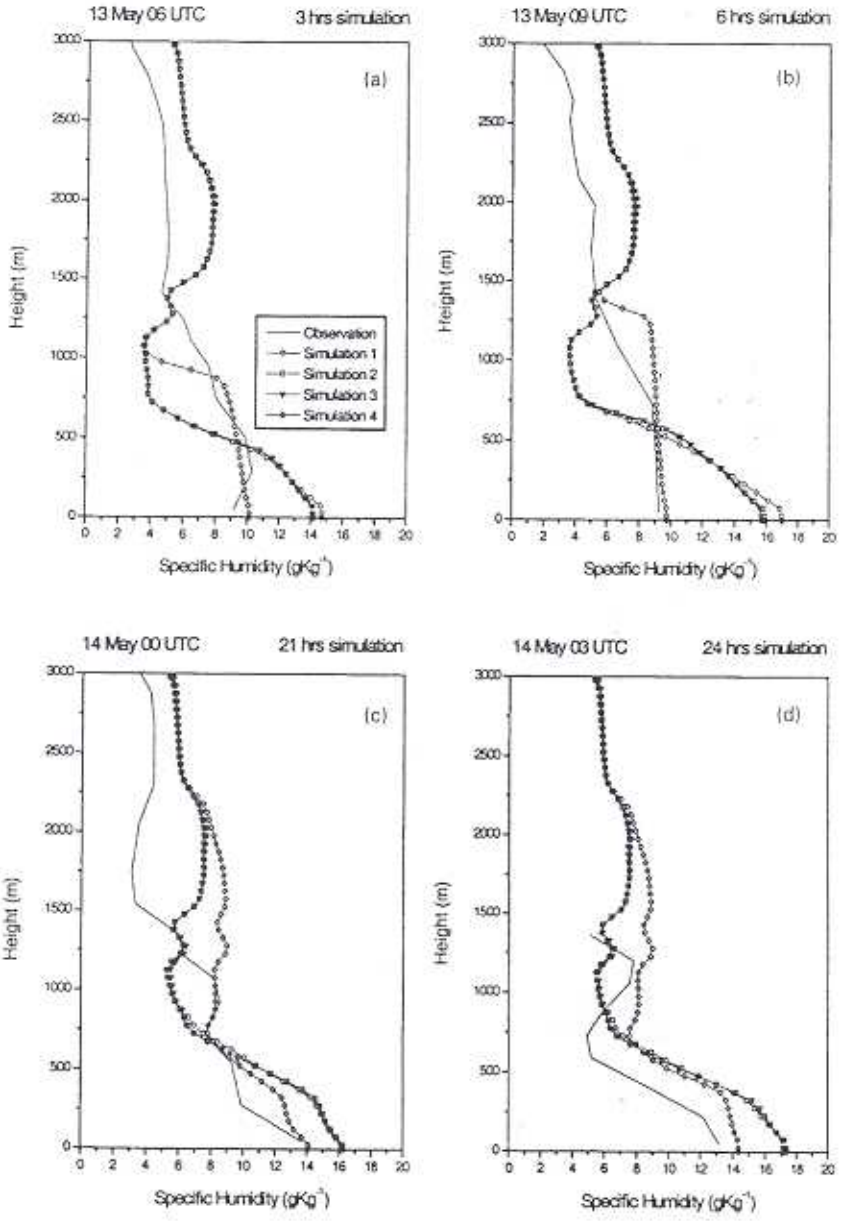

Fig. 9 : Specific humidity profiles - observed and simulated on 13 and 14 May, 1997 at a) 3 hrs, b) 6 hrs, c) 9hrs, d) 21 hrs and e) 24 hrs of simulation.

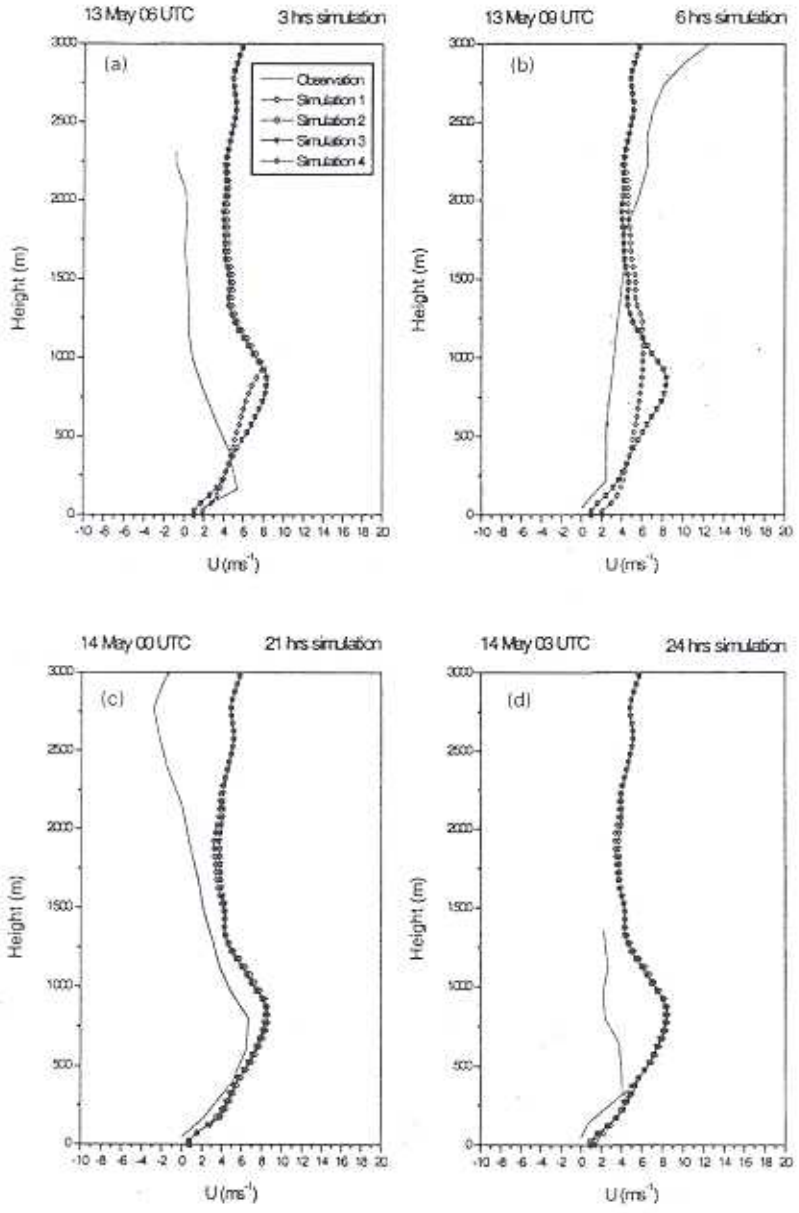

Fig. 10 : Profiles of zonal-wind component - observed and simulated on 13 and 14 May, 1997 at a) 3 hrs, b) 6 hrs, c) 9hrs, d) 21 hrs and e) 24 hrs of simulation.

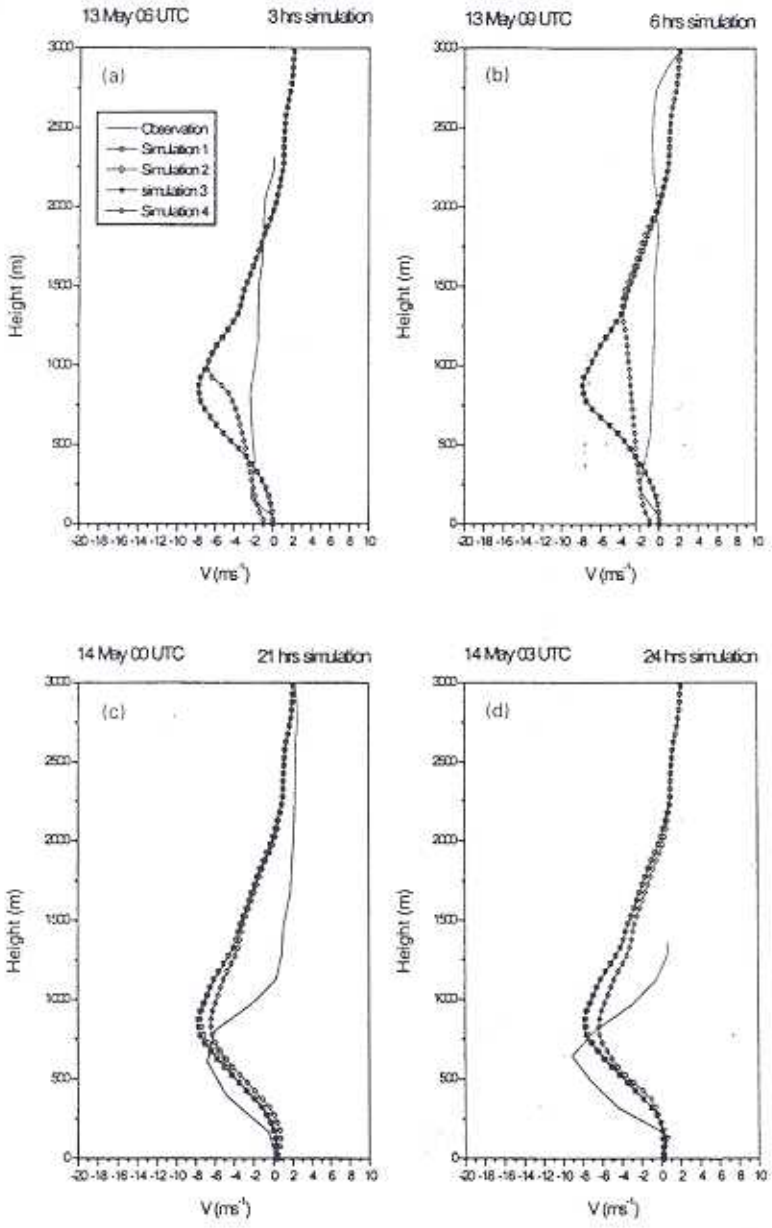

Fig. 11 : Profiles of meridional wind component - observed and simulated on 13 and 14 May, 1997 at a) 3 hrs, b) 6 hrs, c) 9hrs, d) 21 hrs and e) 24 hrs of simulation.

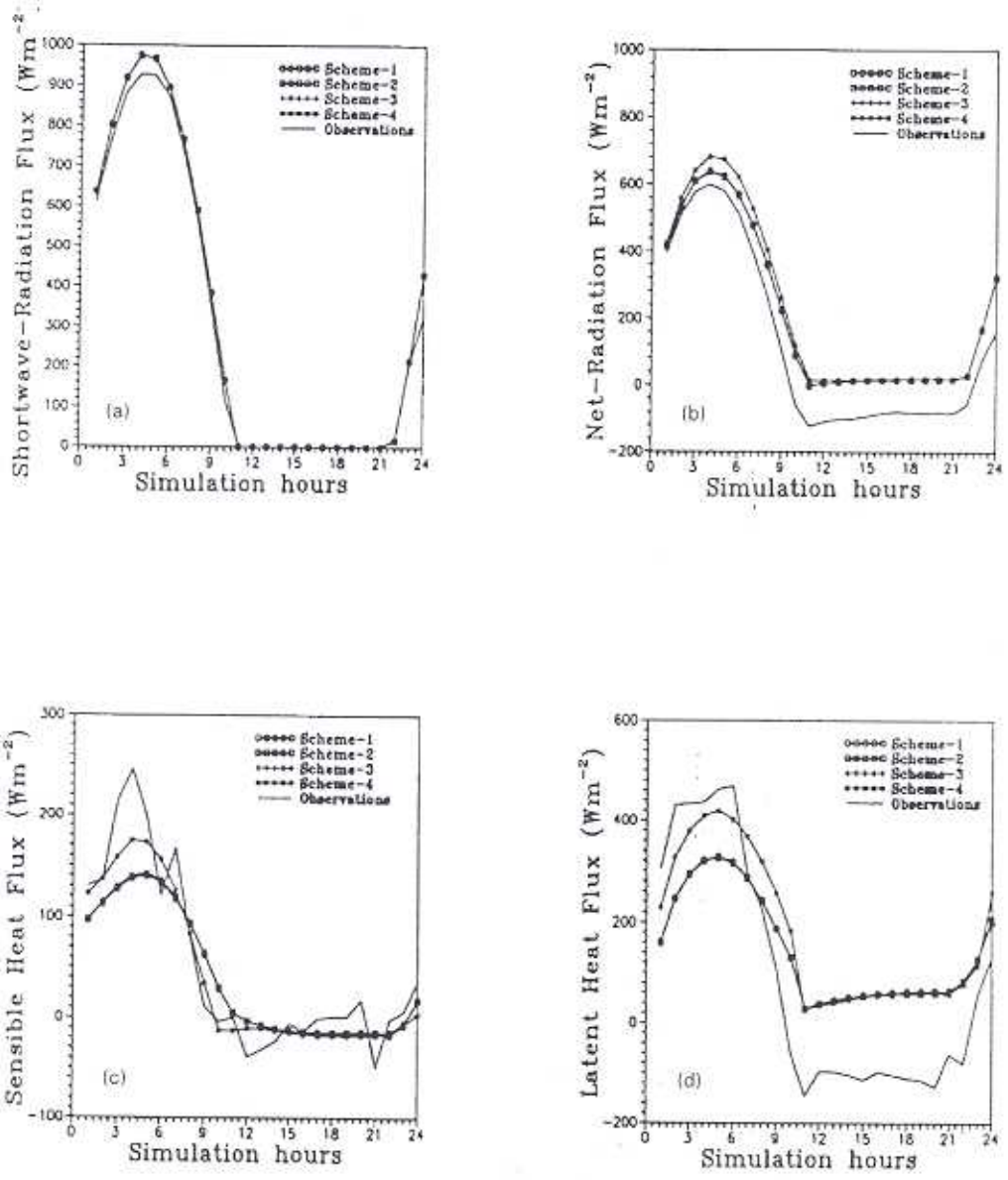

Fig. 12 : Diurnal variation of energy fluxes at surface (a) short wave, (b) net radiation, (c) sensible heat and (d) latent heat starting from 03 UTC 13 May to 03 UTC 14 May,1997.

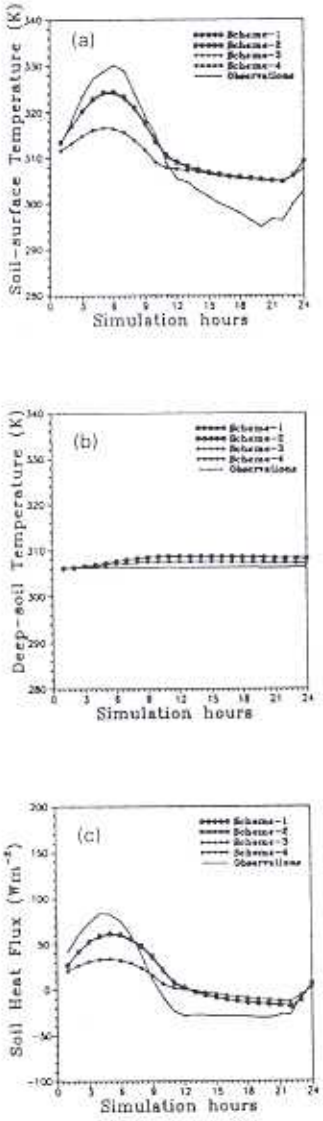

Fig. 13 : Diurnal variation of (a) soil surface temperature, (b) deep-soil temperature and (c) soil heat flux starting from 03 UTC 13 May to 03 UTC 14 May, 1997.

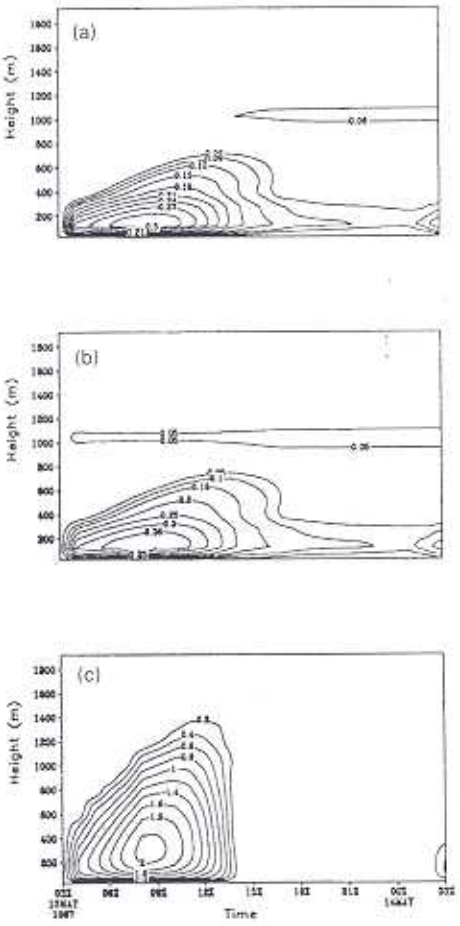

Fig. 14 : The time versus height contour plots of TKE (m^2s^{-1}) with three different subgrid-scale turbulence parameterisation options on 13 and 14 May, 1997. (a) 1.5 order TKE closure scheme of Moeng and Wyngaard, (b) 1.5 order TKE closure scheme of Deardroff and (c) 1.5 order ensemble closure scheme of Sun and Chang.

Table 3 : Overall performance of the models in relation to observations at Anand station.

Parameter	Performance of the model	
	14-15th February (winter)	13-14th May (summer)
Potential temperature (Fig.1 and 8)	In general, model overestimates by 2-4 °K. 21 hr simulation is the closest at all heights. 24 hr is the best prediction above 730 m.	3 hr simulation (2-3 K deviation), and 21 hr simulation above 1 km are the best.
Specific humidity (Fig.2 and 9)	Best are 3 and 21 hr simulations. Break down at 24 hr with underestimates	Fails in simulation. Pattern of profile simulated to some extent.
U-component (Fig.3 and 10)	Best simulation at 3 hr above 1.5 km.	Simulation best up to 800 m; relatively good up to 1.5 km.
V-component (Fig.4 and 11)	Closest in 3 hr simulation 6 hr simulation best up to 1 km	21 hr simulation up to 750 m is good. Beyond this deviation is very large.

temperature profiles show that the simulated potential temperature is less than observation in summer and greater than observed value in winter except during the hours close to sunrise. Apparently no significant difference is found in the diurnal variation of surface fluxes for different SGS closure options. The model under-estimates maximum of latent heat flux whereas overestimates the minimum for both the seasons. In each experiment, although the over all trend of different fluxes are simulated well, the short-wave radiation energy flux and net radiation flux are always overestimated irrespective of seasonal difference (Figs. 5 and 12).

An investigation of the profiles of wind components in Figs. 3-4 and 10-11 demonstrates that the four different simulations give nearly the same characteristics for the PBL structure only with some departure in the late forecast hours. The Figs. 4 and 11 illustrate the fact that the model has a tendency to keep a layer of maximum wind at the same height throughout the day (both in winter and summer) and the meridional wind is influenced more for different parameterisation schemes compared to other variables. Still, the simulations with the closure scheme of Sun and Chang keep a better agreement with observations compared to other schemes. The TKE pattern in Fig. 7 and Fig. 14 show that the ensemble SGS parameterisation of Sun and Chang gives good temporal evolution of PBL structure with a larger TKE maximum. The model responses for two different seasons are explained from the comparison of model simulations with observations, which is summarized in Table-3 and 4.

CONCLUSIONS

Table 4 : Performance of simulated diurnal variations of energy fluxes and soil temperatures at Anand station in summer and winter months.

Parameter	Relative performance with observed data	
	14-15th February (winter)	13-14th May (summer)
Short wave flux (Fig.5 and 12)	Agrees well after 7 hrs.	Simulation good at all hours
Sensible heat flux (Fig.5 and 12)	Simulation good 9 to 16 hrs.	Simulation by method 4 good between 6-12 hrs; later, deviates by 30 Wm^{-2}
Net radiation (Fig.5 and 12)	Simulates well from 6-9 hrs. Does not simulate negative values.	Overestimates by 30 Wm^{-2} in all hrs. by all methods.
Latent heat flux (Fig.5 and 12)	Good simulation for all hrs.	Simulation fails at all hrs.; deviates by 100 Wm^{-2} .
Soil heat flux (Fig.6 and 13)	Fails in simulation of magnitude.	Model fails to simulate; deviate by -50 Wm^{-2} up to 9 hrs. and 30 Wm^{-2} later.
Surface soil temperature (Fig.6 and 13)	Underestimates by 2 °K up to 9 hrs. Overestimates after that by all methods.	Simulation fails though pattern is kept.
Deep soil temperature (Fig.6 and 13)	Simulation good	Gives near results; method 4 is the closest.

The ARPS model performs reasonablywell for the study of PBL structure (Zong *et al.*,1997). The model gives the opportunity to design different experiments with different options available in it.

Seasonal characteristic variation of PBL structure is clearly understood from the model simulations with a simultaneous validation with observational data. The stable thermodynamic structure in the winter month and unstable condition in the summer month is well prescribed by the model. The model also shows the formation of mixing layer within the PBL in the unstable condition in summer. The PBL is drier in February than in May. The amount of moisture decreases very rapidly in the winter month whereas in summer a good amount of moisture is available up to 1 km due to large moisture flux at the surface and good mixing. It is clearly seen that winds are more westerly in summer month and more northerly in winter month that is in good agreement with prevailing synoptic condition at the observational site. Distinguished seasonal characteristics are clearly seen from the maximum and minimum values of the energy fluxes in the PBL (e.g. sensible heat

flux, latent heat flux, short-wave radiation flux, net radiation and soil heat flux). The validation of surface temperature and surface fluxes demonstrates the importance of sophisticated simulation and initialisation of the properties of soil. With the help of observational data an evaluation of performance of four SGS turbulence parameterisation schemes is achieved successfully. The ensemble parameterisation scheme of Sun and Chang appears to be suitable for the PBL over a semi-arid zone. The results prescribe that the subgrid heterogeneity in Eulerian grid model at the time of initialisation may improve the performance of the model. So, a high-resolution 3 dimensional mesoscale model with a grided dataset as its initial condition may perform better for the understanding of PBL characteristics.

ACKNOWLEDGEMENTS

The authors are thankful to India Meteorological Department (IMD) and Indian Institute of Tropical Meteorology (IITM) for providing necessary datasets used for model integration and validation of the results. The authors gratefully acknowledge Prof. Sethu Raman for his valuable suggestions during this study. The authors gratefully acknowledge Department of Science and Technology (DST) for providing partial financial support to carry out this study.

REFERENCES

Arakawa, A. and Lamb, V. R. 1977. Computational Design of the basic dynamical processes of the UCLA general circulation model, Methods in Computational Physics, 17, Academic Press, 174-265, 337.

Batchelor, G. K. 1967. An Introduction to Fluid Dynamics. Cambridge University Press, 615.

Chou, M. D. 1992. A solar radiation model for climate studies. *J. Atmos. Sci.*, 49 : 762-772.

Chou, M. D. and Suarez, M. J. 1994. An efficient thermal infrared radiation parameterisation for use in general circulation models. NASA Tech. Memo., 104606 : 85

Chen, C. 1991. A nested grid, nonhydrostatic, elastic model using a terrain-following coordinate transformation: The radiative-nesting boundary conditions. *Mon. Wea. Rev.*, 119 : 2852-2869.

Coughey, S. J., Wyngaard, J. C. and Kaimal, J. C. 1979. Turbulence in the evolving stable boundary layer. *J. Atmos. Sci.*, 36 : 1041-1052.

Chorbok, G., Raasch, S. and Etling, D. 1992. A comparison of local and non-local turbulence closure methods for the case of a cold air outbreak. *Bound. Layer Meteorol.*, 58 : 69-90.

Deardroff, J. W. 1980. Stratocumulus-capped mixed layers derived from a three-dimensional model. *Bound. Layer Meteorol.*, 18 : 495-527.

Durran, D.R., and Klemp, J.B. 1983. A compressible model for the simulation of moist mountain waves. *J. Atmos. Sci.*, 39 : 2490-2506.

Haltiner, G.J., and William, R.T. 1980. Numerical Prediction and Dynamic Meteorology. John Wiley and Sons. 477.

Holt, T. and Raman, S. 1988. A review and comperative evaluation of multilevel boundary layer parameterisations for the first-order and turbulent kinetic energy closure schemes. *Rev. Geophy.*, 26 : 761-780.

Kain, J. S. and Fritsch, J. M. 1990. A one-dimensional entraining/detraining plume model and its application in convective parameterisation. *J. Atmos. Sci.*, 47: 2784-2802.

Kessler, E. 1969. On the distribution and continuity of water substance in atmospheric circulations. *Meteorol. Monogr. Amer. Meteor. Soc.*, 10 : 84.

Klemp, J. B. and Wilhelmson, R. B. 1978. The simulation of three-dimensional convective storm dynamics. *J. Atmos. Sci.*, 35 : 1070-1096.

Kuo, H. L. 1974.Further studies of the parameterization of the cumulus convection on large-scale flow. *J. Atmos. Sci.*, 31: 1232-1240.

Lilly, D. K. 1962. On numerical simulation of buoyant convection. *Tellus*, 14 : 148-172.

Mellor, G. L. and Yamada, T. 1974. A hierarchy of turbulence closure models for planetary boundary layers. *J. Atmos. Sci.*, 31: 1791-1806.

Ming, X., Droegemeier, K. K., Wong, V., Shapiro, A., and Brewster, K. 1995. Advanced Regional Prediction System, Version 4.0, User's Guide.

Moeng, C.H. and Wyngaard, J. C. 1984. Statistics of conservative scalars in the convective boundary layer. *J. Atmos. Sci.*, 41 : 3161-3169.

Musson-Genon, L.1995. Comparison of different simple turbulence closures with a one-dimensional boundary layer model. *Mon. Wea. Rev.*, 123 : 163-180.

Nagar, S. G., Tyagi, A., Seetaramayya, P. and Singh, S. S. 2000. Evolution of an atmospheric boundary layer at a tropical semi-arid station, Anand during boreal summer month of May - A case study. *Curr. Sci.*, 78(5) : 595-600.

Noilhan, J. and Planton, S. 1989. A simple parameterization of land surface processes for meteorological models. *Mon.Wea. Rev.*, 117 : 536-549.

Noilhan, J., Lacarrere, P. and Bougeault, P. 1991. An experiment with an advanced surface parameterization in a mesobeta-scale model. Part-III: comparison with HAPEX-MOBILHY dataset. *Mon. Wea. Rev.*, 119 : 2393-2413.

Pleim, J. E. and Xiu, A.1995. Development and testing of a surface flux and planetary boundary layer model for application in mesoscale models. *J. Appl. Meteorol.*, 34 : 16-32.

Potty, K. V. J., Mohanty, U.C., Nandi, B., and Ramesh, K.J.1996. Planetary boundary layer over monsoon trough region in a high-resolution primitive equation model. *Proc. Indian Acad. Sci.*, 105 : 339-358.

Satyanarayana, A. N. V., Lykossov, V. N. and Mohanty, U. C. 2000. A study on atmospheric boundary layer characteristics at Anand, India using LSP Experimental data sets. *Bound. Layer Meteorol.*, 96 : 393-419.

Schultz, P. 1995. An explicit cloud physics parameterization for operational numerical weather prediction. *Mon.Wea. Rev.*, 123 : 3331-3343.

Sharman, R. D., Keller, T. L. and Wurtele, M. G. 1988. Incompressible and anelastic flow simulations on numerically generated grids. Mon. Wea. Rev. 116 : 1124-1136.

Smagorinsky, J. 1963. General circulation experiments with the primitive equations. Part I. The basic experiments. *J. Meteorol.*, 14 : 184-185.

Sun, W. Y. and Chang, C. Z. 1986. Diffusion model for a convective layer. Part I: Numerical simulation of convective boundary layer. *J. Climate Appl. Meteorol.*, 25 : 1445-1453.

Yamada, T. 1976. On the similarity functions A, B and C of the planetary boundary layer. *J. Atmos. Sci.*, 33 : 781-793.

Zong, J. and Xu, Q. 1997. The dynamics of cold fronts passing over a quasi-two dimensional isolated mountain ridge. *Tellus*, 49(A): 559-576.